ISSN 0915-633X

NATIONAL INSTITUTE FOR FUSION SCIENCE

Confirmation Method for Metal Plate Penetration of Low Energy Negative Pionlike or Muonlike Particle Beam under Positive Ions

J. Uramoto

(Received - Oct. 7. 1997)

NIFS-531 Dec. 1997

RESEARCH REPORT
NIFS Series

NAGOYA, JAPAN

Confirmation Method for Metal Plate Penetration of Low Energy Negative Pionlike or Muonlike Particle Beam under Positive Ions

Jōshin URAMOTO

National Institute for Fusion Science
332-6 Orosh-cho, Toki-shi, Gifu, 509-52, Japan

Abstract

Negative pionlike or muonlike particles in low energy (< 1000 eV) which are extracted from a H_2 gas discharge, penetrate a metal plate (0.1 cm in thickness) when positive ions exist around the metal plate. By applying a positive bias voltage to the metal plate, the penetration is proved more clearly.

Keywords: negative pionlike particle π^-, negative muonlike particle μ^-, metal plate penetration.

1. Previous Experiment

We have already reported in the previous paper[1] that negative pionlike or muonlike particles are extracted from a H_2 gas discharge in magnetic field.

Schematic diagrams of the previous experimental apparatus are shown in Figs. 1. The apparatus is constructed from a H_2 gas discharge plasma in magnetic fields, three extraction electrodes (with an aperture of 3 mm in diameter) to extract some negatively charged particles and a magnetic mass analyzer (90° deflection-type).

A sheet plasma[2] is produced to generate H^- ions effectively and in wide area. That is, the discharge (cylindrical) plasma flow of about 1 cm in diameter is transformed into a sheet plasma flow of about 3 mm in thickness and about 20 cm in width, while the electron components in the initial discharge plasma are accelerated near 55 eV. The sheet plasma flow enters the electron acceleration anode through the main chamber (50 cm long). A uniform magnetic field of about 50 gauss is applied along the sheet plasma flow in the main chamber where the H_2 gas pressure is about 1.5×10^{-3} Torr. The electron acceleration anode current I_A is 20A. A distance between the sheet plasma center and the first extraction electrode (L) is 7.5 cm. The plasma density in the center of the sheet plasma is about 10^{11}/cc and the electron temperature is about 20 eV. The positive ion density in front of the first extraction electrode is estimated to be about 10^{10}/cc from a positive ion saturation current as H_3^+, while the electron density from the Langmuir probe characteristic is about 10^9/cc and the electron temperature is about 3.0 eV. That is, the electron density in front of the first extraction electrode is reduced near 1/10 of the positive ion density.

The negatively charged particles extracted from the H_2 gas discharge plasma, are injected into the ordinary magnetic mass analyzer (MA) through the slit (3 mm × 1 cm) while each mass of the negatively charged particle is estimated by the following relations: From the analyzing magnetic field B_M where the negative current to the beam collector BC shows a peak, the curvature radius r of the mass analyzer and the extraction (acceleration) voltage V_E, we can estimate the mass m of the negatively charged particle by,

$$m = \frac{Ze\,(B_M r)^2}{2V_E}$$

$$= \frac{8.8 \times 10^{-2}\, Z\,(B_M r)^2\, m_e}{V_E}, \quad \cdots\cdots (1)$$

where e is the electron charge, B_M is in gauss unit, r is in cm unit, V_E is in volt unit and m_e is the electron mass and Z is the charge number. For the curvature radius $r = 4.3$ cm of this mass analyzer, the Eq. (1) is rewritten by

$$m = \frac{1.63\ Z\ B_M{}^2}{V_E} m_e. \quad \text{..... (2)}$$

In the extraction of negatively charged particles, the first extraction electrode (L) is electrically floated, whose potential V_L is about −10V with respect to the electron acceleration anode. A potential V_M of the second extraction electrode (M) is kept at 300V or 75V. A potential V_E of the final extraction electrode (E) is 800V.

In this experiment, it is noted that the back space of the beam collector is shielded[3] perfectly from the diffusion of positive ions as shown in Fig. 1 (B). The dependences of the negative current I^- to the beam collector on the analyzing magnetic field B_M are shown in Figs. 2 (A) and 2 (B) for the beam collector potential $V_{BC} = 0$V and $V_{BC} = 75$V. Obviously, in a case (1) of Fig. 2 (A) or Fig. 2 (B) at the second extraction electrode potential $V_M = 300$V, a peak of I^- at the analyzing magnetic field $B_M \approx (4.0 \times 240)$ gauss = 960 gauss is corresponding to H^- ion, assuming that Z = 1 in Eq. (2). That is, we obtain $m \approx 1880\ m_e$ (near the true mass of $H^- = 1842\ m_e$) as $V_E = 800$V. Then, we find that another main peak of I^- at $B_M \approx (1.54 \times 240)$ gauss ≈ 370 gauss is corresponding to a negative pion, assuming that Z = 1 in Eq. (2). That is, we obtain $m \approx 278\ m_e$ (near the true pion mass = 273 m_e) as $V_E = 800$V.

In another case (2) of Fig. 2 (A) or Fig. 2 (B) at $V_M = 75$V, a peak of I^- at $B_M \approx 960$ gauss is also corresponding to H^- ion. Then, we find that another main peak of I^- at $B_M \approx (1.33 \times 240)$ gauss ≈ 320 gauss is corresponding to a negative muon, assuming that Z = 1 in Eq. (2). That is, we obtain $m \approx 209\ m_e$ (near the true muon mass = 207 m_e) as $V_E = 800$V.

A special peak e_H of I^- is observed at $B_M \approx (0.6 \times 240)$ gauss = 144 gauss as seen in Figs. 2 (A) or 2 (B). We consider that this peak e_H is caused by high energy electrons which come directly from the outside of the sheet plasma. Because the e_H peak position of B_M does not depend on the final extraction voltage V_E while the H^-, π^-, μ^- peaks depend exactly on V_E in Eq. (2). The energy eV_H of high energy electron e_H is estimated to be $eV_H \approx 33.8$ keV, if we take $m = m_e$, $V_E = V_H$ and $B_M \approx 144$ gauss at the e_H peak in Eq. (2).

When a positive potential $V_{BC} = 75V$ is applied to the beam collector BC, their peaks of I^- increase, as seen in Fig. 2 (B), about 1.3 times for H^- ion, about 200 times for π^- or μ^- and about 50 times for e_H. These large apparent increments of negative current peaks under the positive potential $V_{BC} > 0$ of the beam collector BC, have been explained by a mechanism due to positive ions within the mass analyzer MA and secondary electrons inside BC.[1)]

2. Experiment of Metal Plate Penetration

Schematic diagrams of this experimental apparatus are shown in Fig. 3 and Figs. 4 (A) and (B). It is different from the previous experimental apparatus[1)] that only a metal plate MP (0.1 cm in thickness) is arranged in front of the beam collector BC within the mass analyzer MA while a bias voltage V_{MP} is applied to the metal plate MP. (A potential V_M of the second extraction electrode (M) is kept at 75V corresponding to a case of the negative muonlike particle μ^-).

Dependences of negative currents to BC (I^-) and MP (I_{MP}^-) on the analyzing magnetic field B_M are shown in Fig. 5 under the beam collector bias voltage $V_{BC} = 75V$, where the bias voltage V_{MP} of MP is 0V or 100V. Then, the H^- ion currents appear for only the metal plate MP. On the other hand, the apparent negative muonlike particle currents as shown in Fig. 2 (B), appear for only the beam collector BC around $B_M \approx 1.3 \times 240$ gauss. It should be noted that I^- to BC much increases at the higher bias voltage $V_{MP} = 100V$ of MP. A dependence of the peak current I_P^- (as shown in Fig. 5) on V_{MP} is shown in Fig. 6 with I_{MP}^- to MP. The I_P^- increases abruptly for $V_{MP} >$ 40V. It should be noted also that the I_{MP}^- is very small in comparison to I_P^- even if V_{MP} much increases above $V_{BC} = 75V$.

A dependence of the net negative muonlike particle current I^- to BC (under $V_{BC} = 0V$) on B_M is shown in Fig. 7 with the I_{MP}^- (at $V_{MP} = 0V$). Similarly, no current peaks of I_{MP}^- appear around $B_M \approx 1.3 \times 240$ gauss while only a current peak of the high energy electron e_H appears near $B_M \approx 0.6 \times 240$ gauss as seen in Figs. 2. From these experimental results, we can conclude that the negative muonlike particles penetrate a metal plate. Similar experimental results are confirmed also for the negative pionlike particles under the second extraction voltage $V_M = 300V$. Thus, we conclude that the negative pionlike or muonlike particles can penetrate a metal plate if positive ions exists around the metal plate. The positive ions are generated secondarily from the incidence of the H^- ion beam to the back metal plate BMP of MA as shown in Figs. 8 (A) and (B).

In the next experiment, the back metal plate BMP is removed from the mass analyzer MA as shown in Figs. 9 (A) and (B). Thus, the positive ions around the metal plate MP are reduced abruptly. Under this condition, dependences of the negative currents I^- (to BC) and I_{MP}^- (to MP) on B_M are shown in Figs. 10 (A) and 10 (B) at $V_{MP} = 0V$ or $V_{MP} = 100V$ and $V_{BC} = 0V$ or $V_{BC} = 75V$. As expected, no negative current peaks of I^- appear around the $B_M \approx 1.3 \times 240$ gauss corresponding to the negative muonlike particle beam while net negative current peaks of I_{MP}^- are observed near the $B_M \approx 1.3 \times 240$ gauss. From these results, we conclude that the negative muonlike or pionlike particle beam can not penetrate the metal plate MP without the positive ions around MP.

3. Discussion I

The fact that I^- peak much increases for $V_{MP} > 40V$ as seen in Fig. 6, can be related with increment of the positive ion effects when the back ground low energy electrons are removed by the positive bias voltage $V_{MP} > 40V$.

To prove the above expectation, a side metal plate SP is arranged as shown in Figs. 11 (A) and (B) near the beam collector BC. Thus, dependences of I^- (to BC) on B_M under $V_{BC} = 75V$ are shown in Fig. 12 for the two bias voltages V_{SP} of SP. Obviously, the peak current I_P^- of I^- increases abruptly when V_{SP} increases from 25V to 100V. Then, the H^- ion current does not increase. In Fig. 13, dependences of the peak current I_P^- (corresponding to the negative muonlike particle beam) and the I_H^- (corresponding to H^- ion beam) on V_{SP} are shown with the negative current I_S^- to the side metal plate SP. The I_S^- is very small in comparison with the I_P^- and the I_H^-. However, the I_P^- much increases with V_S. We consider that this increment of I_P^- is arised by removement of the back ground low energy electrons due to the positive bias voltage $V_{SP} > 0$. That is, the large increment of I_P^- can be related with increment of the positive ion effects. On the other hand, the H^- ion current peak I_H^- is constant for $V_{SP} > 0$. These facts show that the secondary electrons due to the decay of the negative muonlike particles μ^- are very great in number in comparison with those due to the H^- ions. Therefore, the charge compensation of the secondary electrons due to μ^- decay needs a large charge effect of positive ions which are not compensated by the back ground low energy electrons within MA.

In relation with the above experimental fact, it should be noted that the metal plate MP of the

penetration experiment in Figs. 4 also removes the back ground low energy electrons in front of the beam collector when a positive bias voltage $V_{MP} > 0$ is applied to MP.

4. Discussion II

According to the ordinary collision energy loss theory, the unit energy loss inside the metal plate for the typical negative pion or muon is extremely large (above 10 MeV/cm for Cu). Thus, it is considered theoretically that the negative pionlike or muonlike particle around the energy of 800 eV can not penetrate the metal plate MP of 0.1 cm in thickness. However, two experimental conditions in our experiment are different from the ordinary theory. The one is that positive ions exsist around the metal plate when the negative pionlike or muonlike particles penetrate it. The other one is that the negative pionlike or muonlike particle velocity υ_π or υ_μ is very small in comparison with electron velocities υ_e in atomic orbits. That is,

$$\upsilon_\pi \text{ or } \upsilon_\mu < \upsilon_e, \cdots\cdots$$

because $\upsilon_\pi \approx 1.1 \times 10^8$ cm/sec or $\upsilon_\mu \approx 1.3 \times 10^8$ cm/sec at an energy of 800 eV and the orbital electron velocity $\upsilon_e \approx 2.7 \times 10^8$ cm/sec as a bound energy 20 eV in atom. Therefore, the collisional energy losses due to their electrons in the metal plate MP are much reduced[4] while the ordinary theory is not applied to our experiment.

The characteristics for metal plate penetration of a low energy negative pionlike or muonlike particle beam have been already[5] reported in another case using an electron beam.

When an insulator plate is arranged in stead of the metal plate, the characteristics of the negative current I^- corresponding to the negative pionlike or muonlike particle is near those under the bias voltage of MP $V_{MP} = 0V$. Moreover, even if the thickness of MP is increased from 0.1 cm to about 0.5 cm, the penetration characteristics is the same almost.

References

1) J. Uramoto: National Institute of Fusion Science, Nagoya, Japan-Research Report, NIFS-To be reported.

2) J. Uramoto: Journal of the vacuum society of Japan, **27** (1984) 610 in Japanese.

3) J. Uramoto: NIFS-400 (1996).

4) Nuclear Physics by Enrico Fermi, by The University of Chicago press (1950).

5) J. Uramoto: NIFS-350 (1995).

Figure Captions

Fig. 1 (A) Schematic diagram of previous experimental apparatus.

1: Cylindrical plasma in discharge anode. 2: Discharge cathode. 3: H_2 gas flow. 4: Discharge power supply. 5: Electron acceleration power supply. 6: Vacuum pump. 7: Area where cylindrical plasma is transformed into sheet plasma. 8: Insulation tube. 9: A pair of permanent magnets. 10: Magnetic field coils. 11: Electron acceleration anode. I_A: Current to electron acceleration anode. CP: Cylindrical plasma. SP: Sheet plasma. B_Z: Magnetic field. L: First extraction electrode. M: Second extraction electrode. E: Final extraction electrode. V_M: Potential (variable) of second extraction electrode with respect to electron acceleration anode. V_E: Potential (800V) of final extraction electrode with respect to electron acceleration anode. MA: Magnetic deflection (90°) mass analyzer. B_M: Magnetic field intensity of MA. BC: Beam collector of MA. V_{BC}: Positive potential of BC with respect to MA. I^-: Negative current to BC. $H\bar{0}$: Hydrogen negative ions outside of sheet plasma. H^-: Accelerated hydrogen negative ions. $\pi\bar{0}$: Negative pionlike particles outside of sheet plasma. π^-: Accelerated negative pionlike particles.

Fig. 1 (B) Schematic diagram of mass analyzer.

S: Entrance slit position. X: Entrance of uniform magnetic field.

Ins: Insulator behind BC. + Ion: Positive ions in front of BC. Fe: shows Iron.

Fig. 2 (A) Dependences of negative current I^- to BC on magnetic field intensity B_M of MA under beam collector potential $V_{BC} = 0V$.

(1): Potential of second extraction electrode $V_M = 300V$. (2): $V_M = 75V$. H^-: Peak of I^- corresponding to hydrogen negative ion. π^-: Peak of I^- corresponding to negative pionlike particle. μ^-: Peak of I^- corresponding to negative muonlike particle. e_H: peak of I^- corresponding to high energy electron.

Fig. 2 (B) Dependence of I^- to BC on B_M of MA under $V_{BC} = 75V$.

(1): $V_M = 300V$. (2): $V_M = 75V$. H^-, π^-, μ^-, e_H: See captions of Fig. 2 (A).

Fig. 3 Schematic diagram of experimental apparatus for metal plate penetration.

MP: Metal (Cu) plate (1.5 cm × 1.5 cm and 0.1 cm in thickness). BC: Beam collector (0.5 cm × 1.0 cm).

[See Figure caption of Fig. 1 (A)].

Figs. 4 (A) and (B) Schematic diagrams of mass analyzer MA for metal plate penetration experiment.

B_M: Analyzing magnetic field. MP: Metal plate. V_{MP}: Bias voltage of MP with respect to MA. I_{MP}^-: Negative current to MP. μ^-: Negative muonlike particle. e_H: High energy electron. C: Magnetic coils of MA. (N): North pole of electro-magnet. (S): South pole.

[See Figure captions of Fig. 1 (A) and Fig. 1 (B)].

Fig. 5 Dependences of negative currents I^- to BC and I_{MP}^- to MP on analyzing magnetic field B_M under metal plate bias voltage V_{MP} = 0V or 100V.

Beam collector bias voltage: V_{BC} = 75V. μ^-: Negative current corresponding to negative muonlike particle. H^-: Negative current corresponding to H^- ion. I_P^-: Negative current peak corresponding to negative muonlike particle.

Fig. 6 Dependence of negative current peak I_P^- (in Fig. 5) and negative current I_{MP}^- (near B_M = 1.3 × 240 gauss in Fig. 5) on V_{MP}.

Fig. 7 Dependences of net negative currents I^- (under V_{BC} = 0V) and I_{MP}^- (under V_{MP} = 0V) on B_M.

μ^-: Net negative current corresponding to negative muonlike particle. e_H: Net high energy electron current to MP. H^-: Net H^- ion current to MP.

Figs. 8 (A) and (B) Schematic diagrams of mass analyzer with back metal plate BMP.

H+: Hydrogen positive ion generated secondarily from H^- ion.

[See Figure captions of Fig. 1 (A) and Fig. 1 (B)].

C: Magnetic coil of MA. (N): North pole of electro-magnet. (S): South pole.

Figs. 9 (A) and 9 (B) Schematic diagrams of mass analyzer MA for metal plate penetration experiment in a case without back metal plate BMP of MA.

[See Figure caption of Figs. 4 (A) and (B)].

Fig. 10 (A) Dependences of negative current I^- (to BC) on B_M in a case without BMP.

V_{BC}: Bias voltage of BC. V_{MP}: Bias voltage of MP. (1): $V_{BC} = 0V$ and $V_{MP} = 0V$. (2): $V_{BC} = 0V$ and $V_{MP} = 100V$. (3): $V_{BC} = 75V$ and $V_{MP} = 0V$. (4): $V_{BC} = 75V$ and $V_{MP} = 100V$.

Fig. 10 (B) Dependence of negative current I_{MP}^- (to MP) on B_M in a case without BMP.

(1): $V_{BC} = 0V$ and $V_{MP} = 0V$. (2): $V_{BC} = 0V$ and $V_{MP} = 100V$. e_H: Current peak corresponding to high energy electron. μ^-: Current peak corresponding to negative muonlike particle.

Fig. 11 Schematic diagrams of mass analyzer MA under arrangement of side metal plate SP.

V_S: Bias voltage of SP with respect to MA. I_S^-: Negative current to SP.

(See Figure captions of Fig. 3 and Figs. 4).

Fig. 12 Dependences of negative current I^- (to BC) on B_M under arrangement of SP at $V_{BC} = 75V$.

V_S: Bias voltage of SP. (1): $V_S = 25V$. (2): $V_S = 100V$. I_P^-: Current peak corresponding to negative muonlike particle μ^-. I_H^-: Current peak of H^- ion.

Fig. 13 Dependences of I_P^-, I_H^- and I_S^- (current to SP) on V_S (bias voltage of SP).

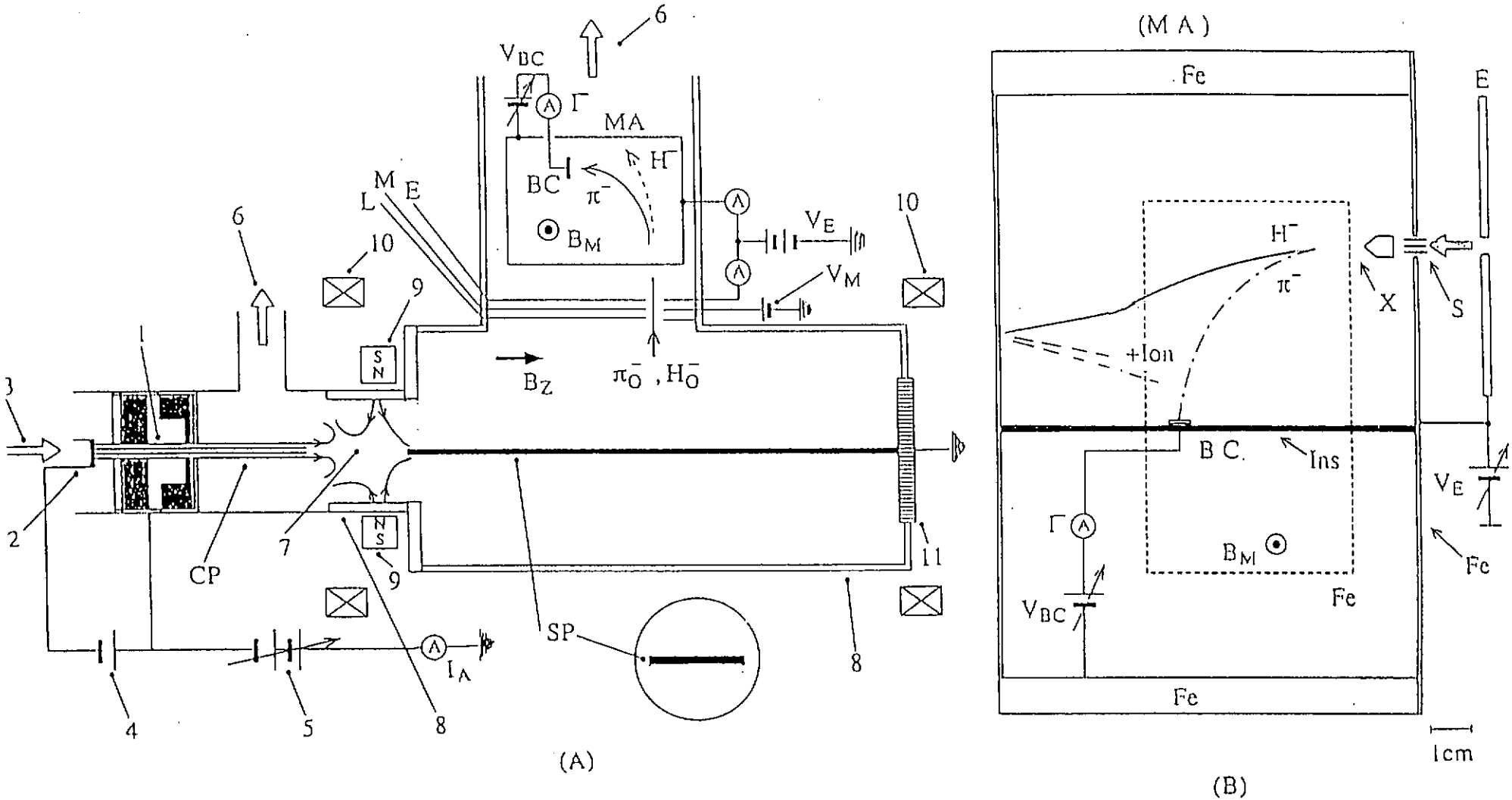
6
V_{BC}
Γ
MA
H^-
BC
π^-
B_M
M
L
E
V_E
V_M
10
9
B_Z
π_O^- , H_O^-
3
1
2
CP
7
S
N
N
S
9
11
SP
8
I_A
4
5
8
(A)
(M A)
Fe
E
H^-
π^-
X
S
+Ion
B C.
Ins
V_E
Γ
B_M
Fe
Fe
V_{BC}
Fe
1cm
(B)

Fig. 1

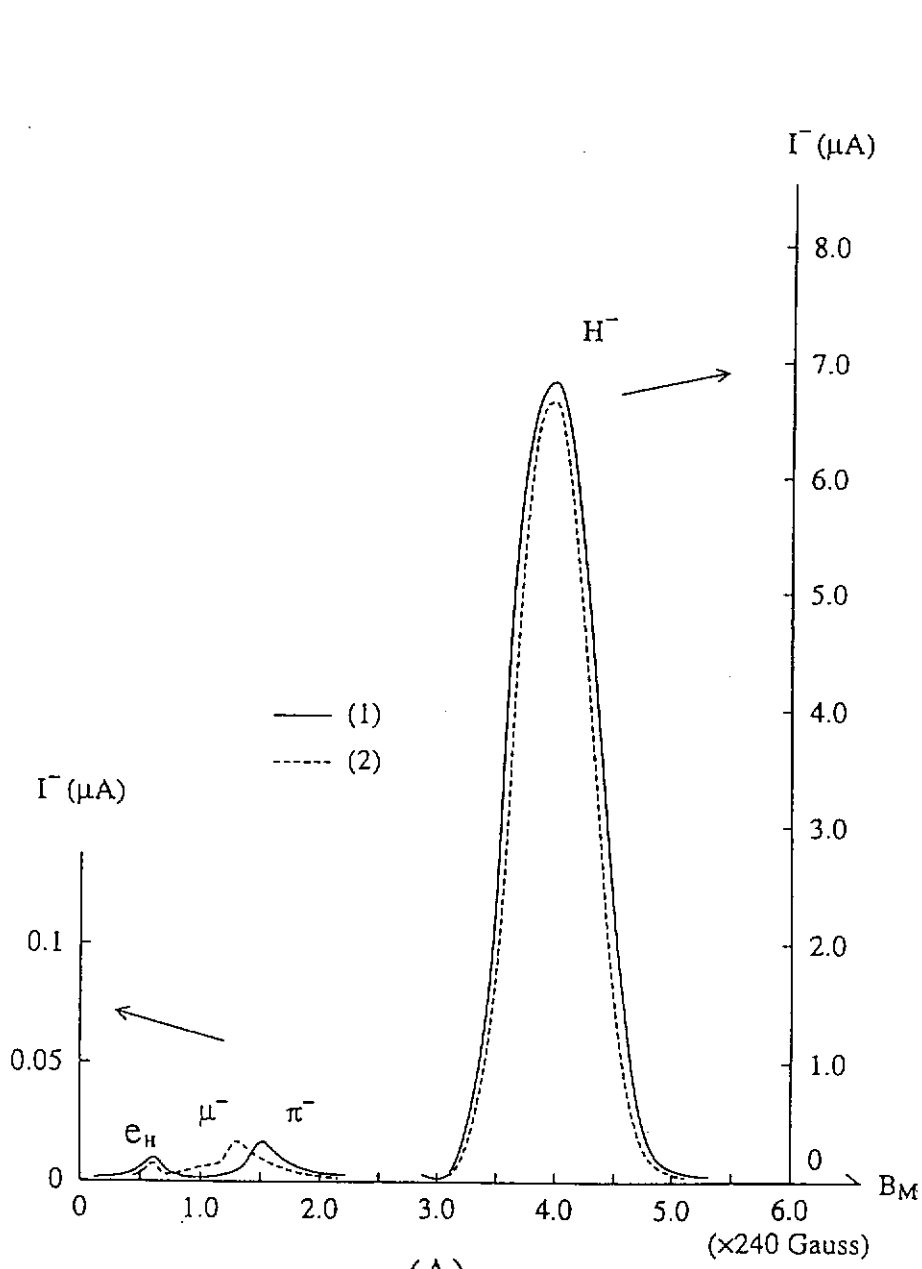
I⁻ (μA)
I⁻ (μA)
H⁻
(1)
(2)
0.1
0.05
0
eн
μ⁻
π⁻
8.0
7.0
6.0
5.0
4.0
3.0
2.0
1.0
0
0
1.0
2.0
3.0
4.0
5.0
6.0
BM
(×240 Gauss)

(A)

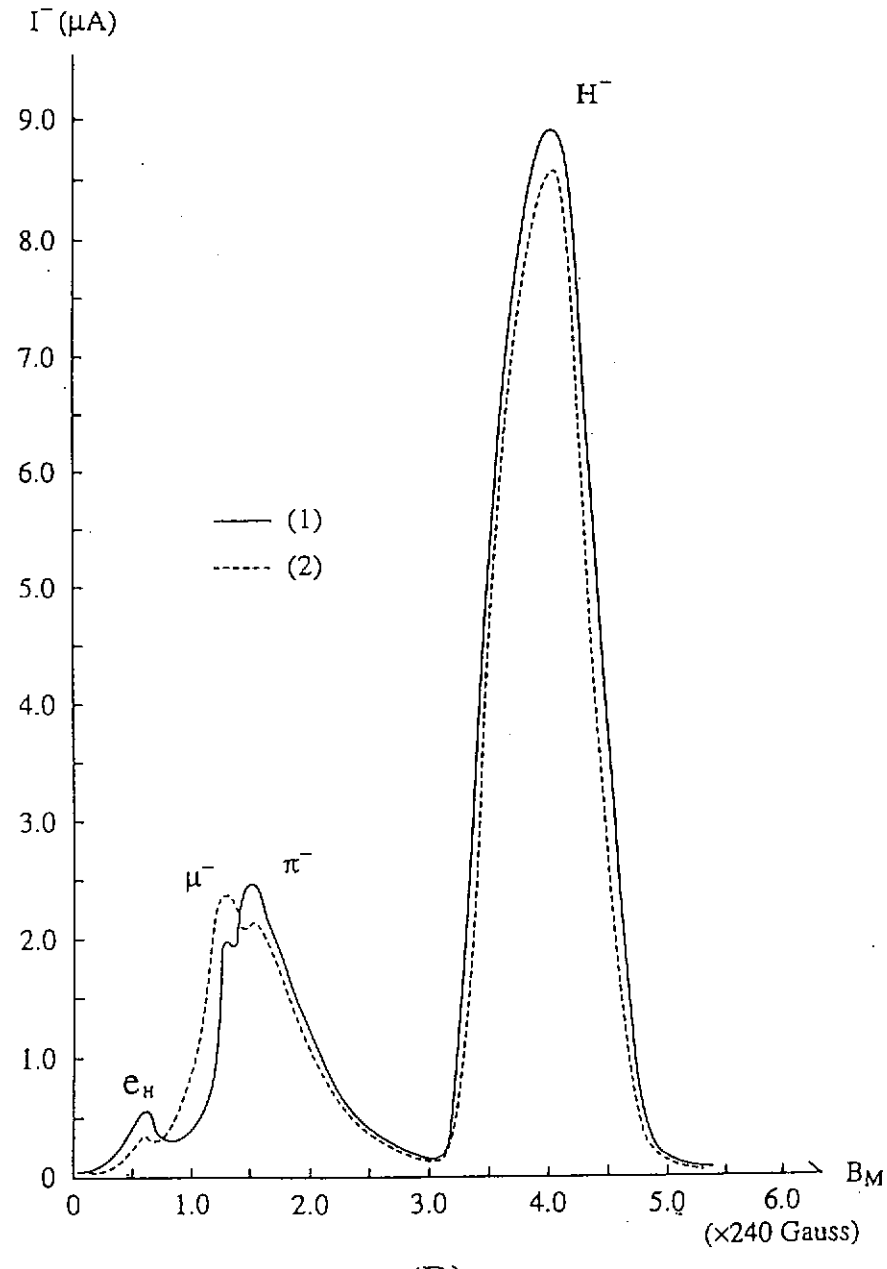
I⁻ (μA)
H⁻
9.0
8.0
7.0
6.0
5.0
4.0
3.0
2.0
1.0
0
(1)
(2)
μ⁻
π⁻
eн
0
1.0
2.0
3.0
4.0
5.0
6.0
BM
(×240 Gauss)

(B)

Fig. 2

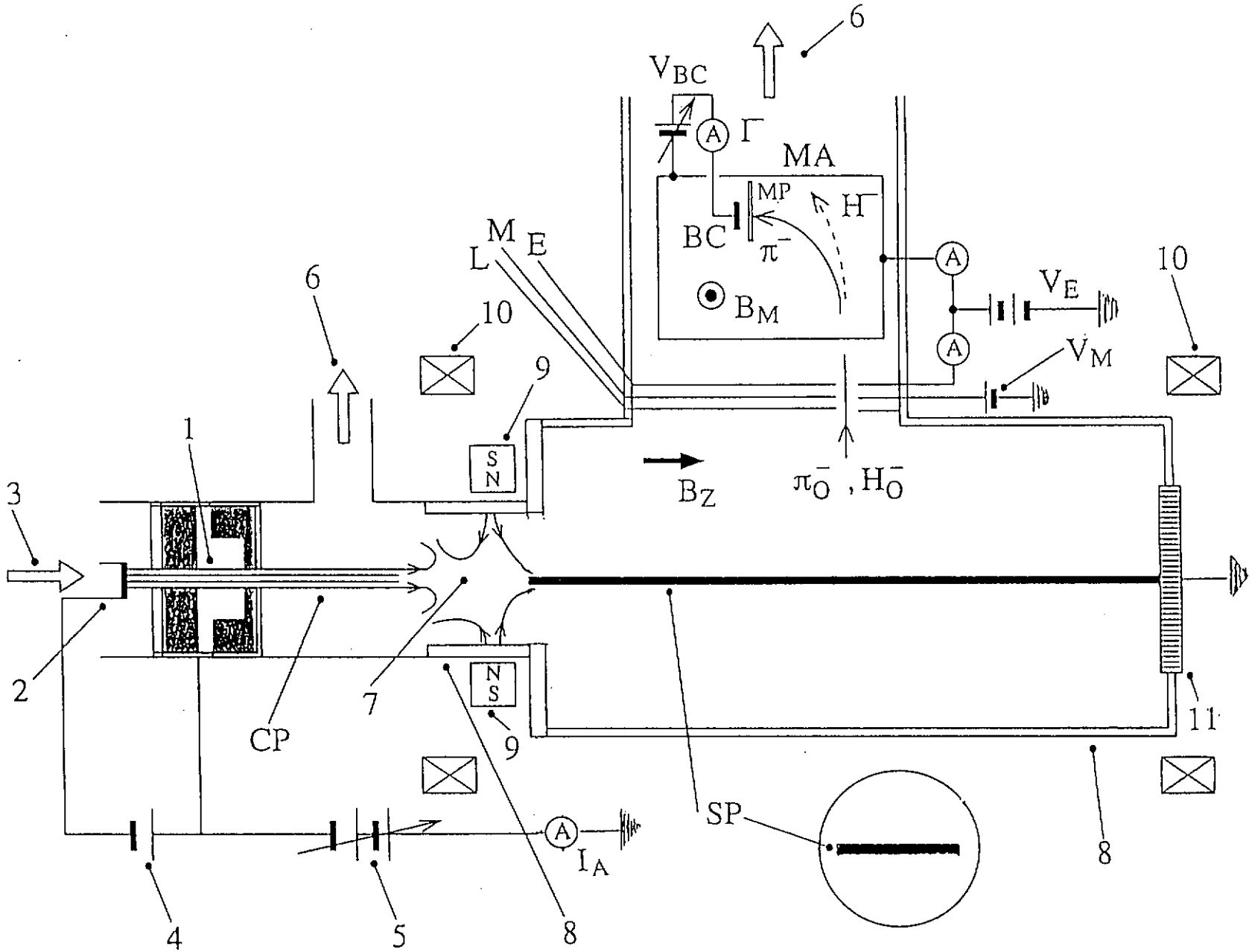
6
V_{BC}
A
Г
MA
MP
H⁻
BC
π⁻
M
L
E
B_M
A
V_E
A
V_M
10
10
6
9
1
S
N
B_Z
π_O^- , H_O^-
3
2
CP
7
N
S
9
11
SP
8
A
I_A
4
5
8

Fig. 3

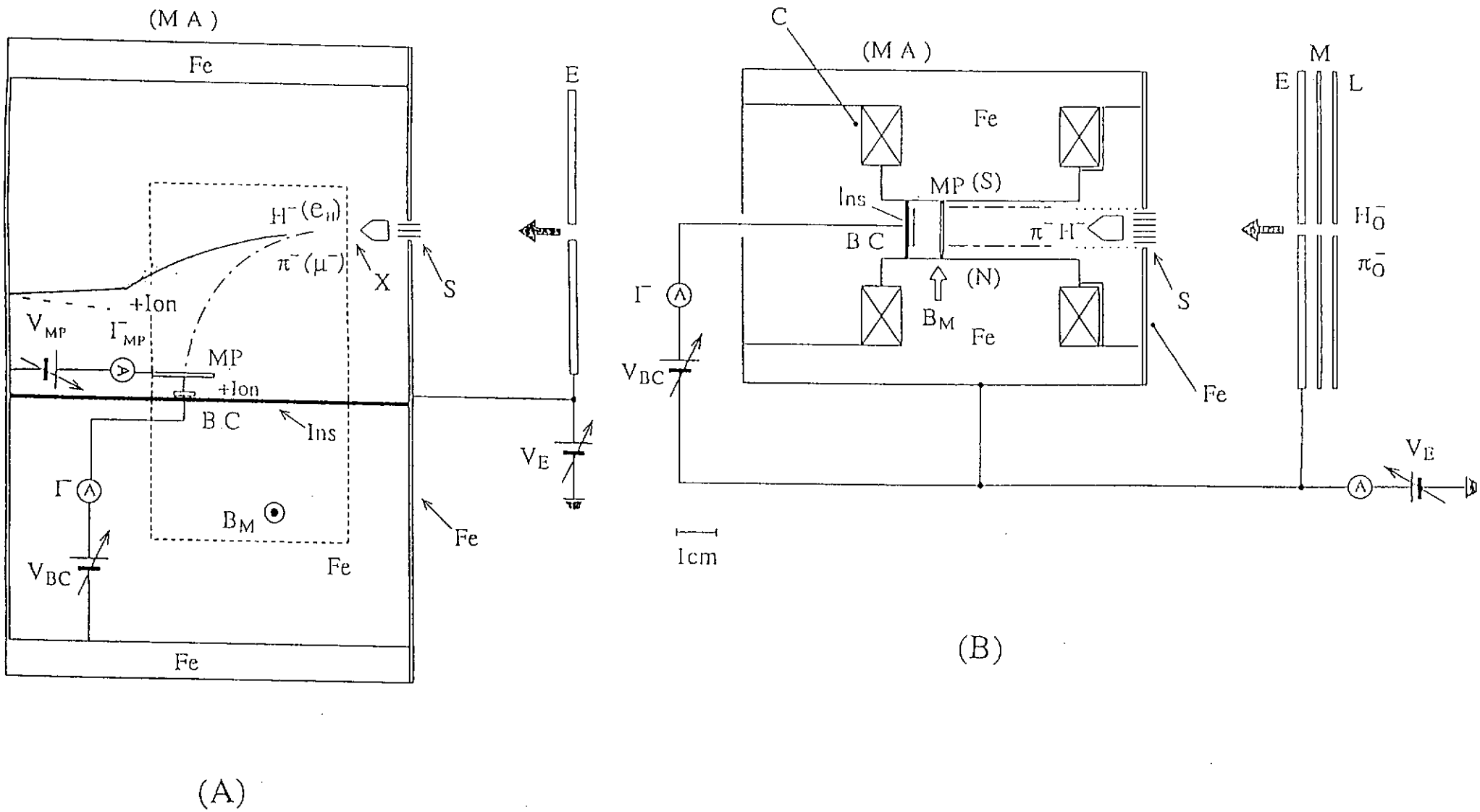
(M A)
Fe
E
$H^-(e_n)$
$\pi^-(\mu^-)$
X
S
+Ion
V_{MP}
I^-_{MP}
MP
+Ion
B C
Ins
I^-
V_{BC}
B_M
Fe
Fe
Fe
V_E
(A)
C
(M A)
Fe
MP (S)
Ins
B C
$\pi^- H^-$
(N)
B_M
Fe
S
Fe
I^-
V_{BC}
1cm
M
E
L
H_O^-
π_O^-
V_E
(B)

F i g . 4

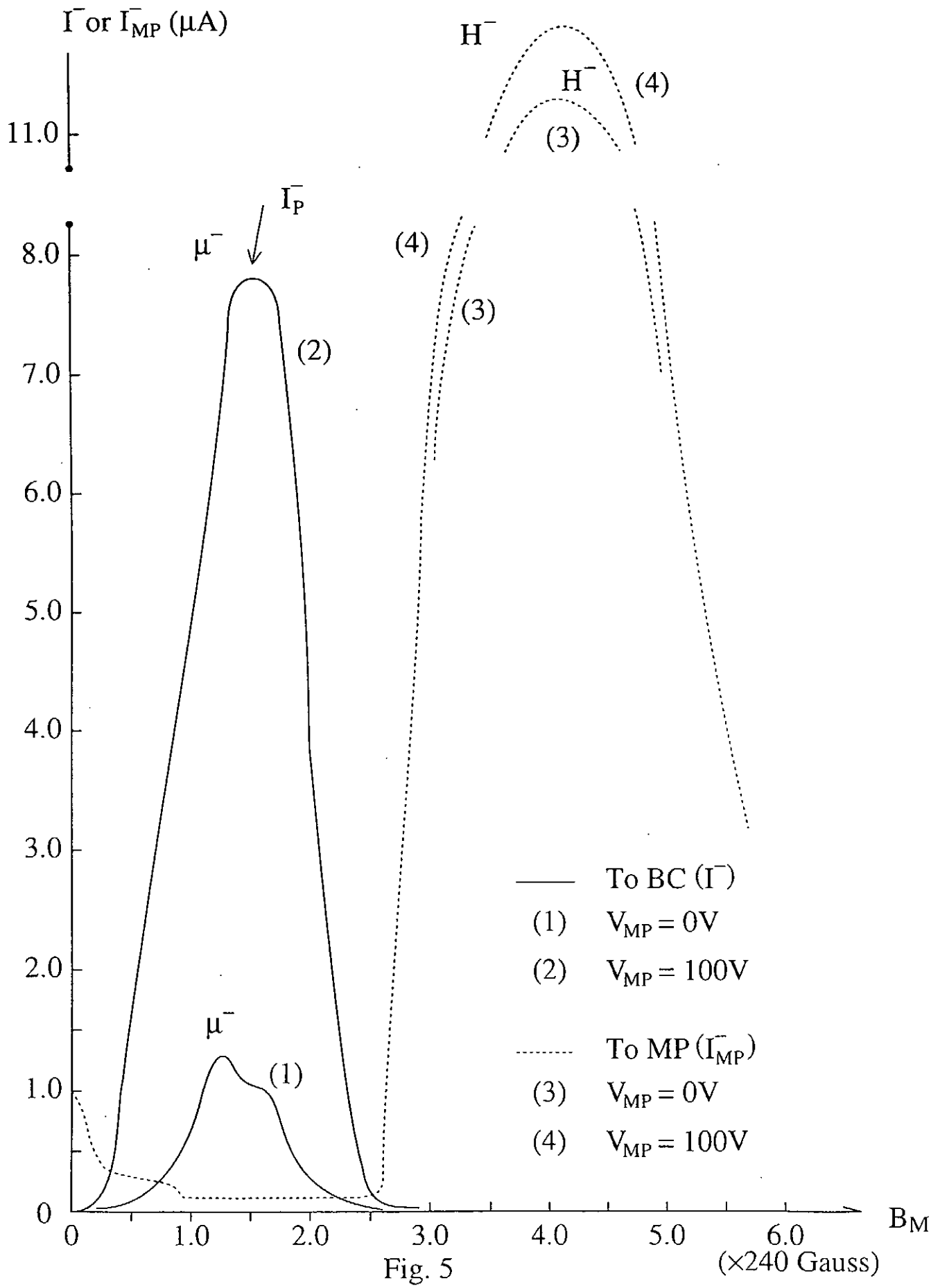
I⁻ or I⁻MP (μA)
11.0
8.0
7.0
6.0
5.0
4.0
3.0
2.0
1.0
0
H⁻
H⁻
(4)
(3)
I⁻P
μ⁻
(4)
(3)
(2)
μ⁻
(1)
To BC (I⁻)
(1) VMP = 0V
(2) VMP = 100V
To MP (I⁻MP)
(3) VMP = 0V
(4) VMP = 100V
0
1.0
2.0
3.0
4.0
5.0
6.0
BM
(×240 Gauss)

Fig. 5

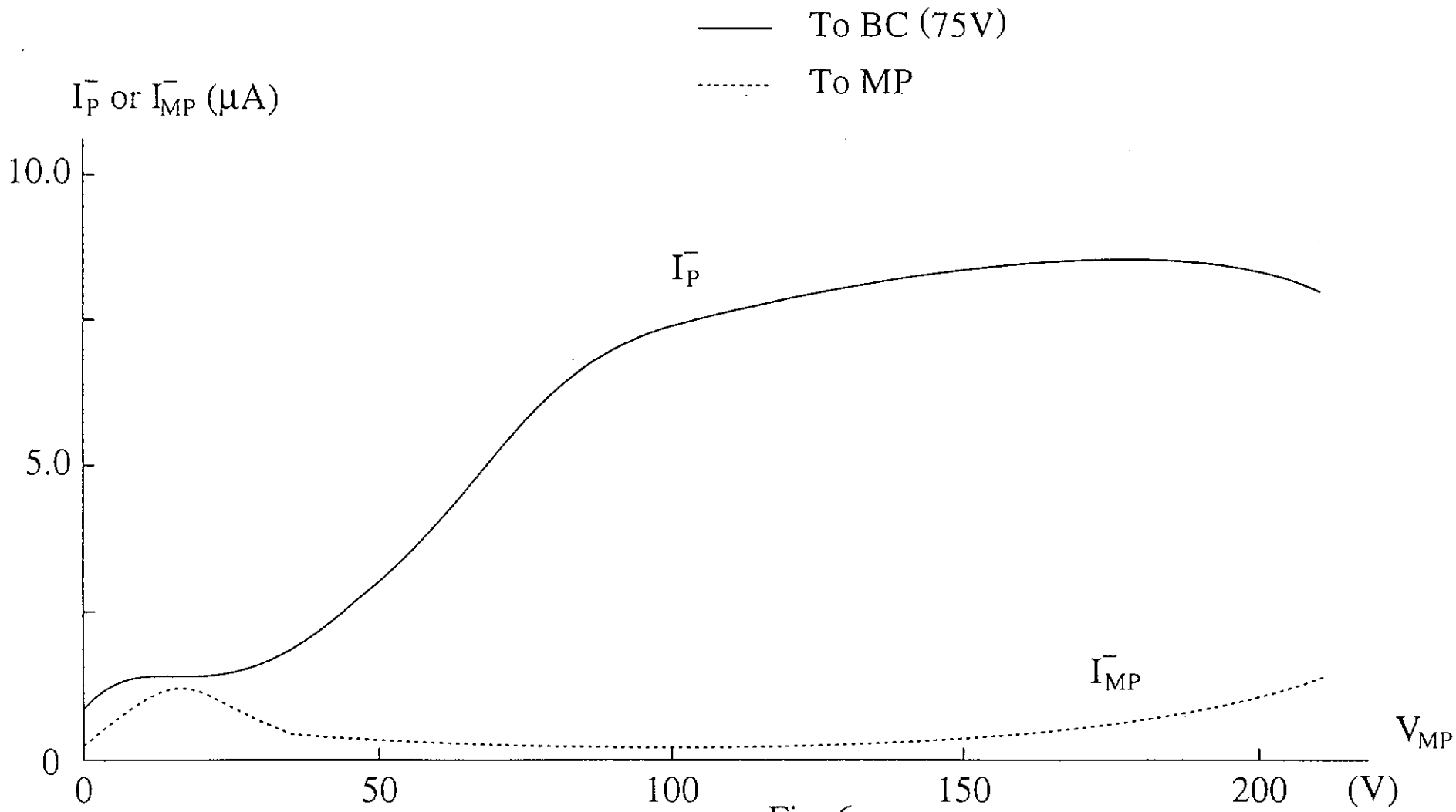
To BC (75V)
To MP
$\bar{I}_P$ or $\bar{I}_{MP}$ (μA)
10.0
5.0
0
$\bar{I}_P$
$\bar{I}_{MP}$
V_{MP}
0
50
100
150
200
(V)

Fig. 6

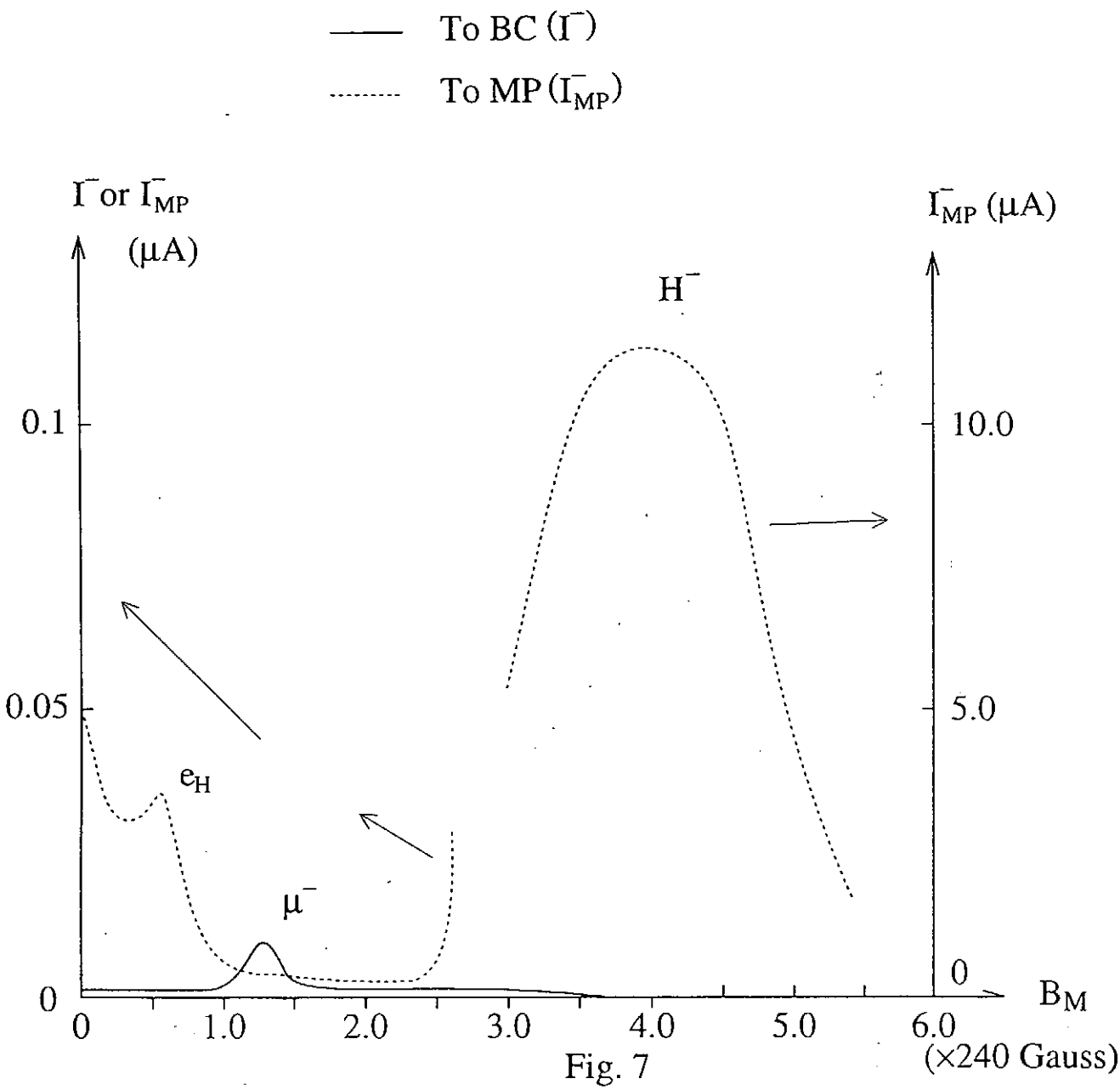
To BC (I^-)
To MP (I^-_{MP})
I^- or I^-_{MP} (μA)
I^-_{MP} (μA)
H^-
0.1
0.05
0
10.0
5.0
0
e_H
μ^-
0
1.0
2.0
3.0
4.0
5.0
6.0
B_M
(×240 Gauss)

Fig. 7

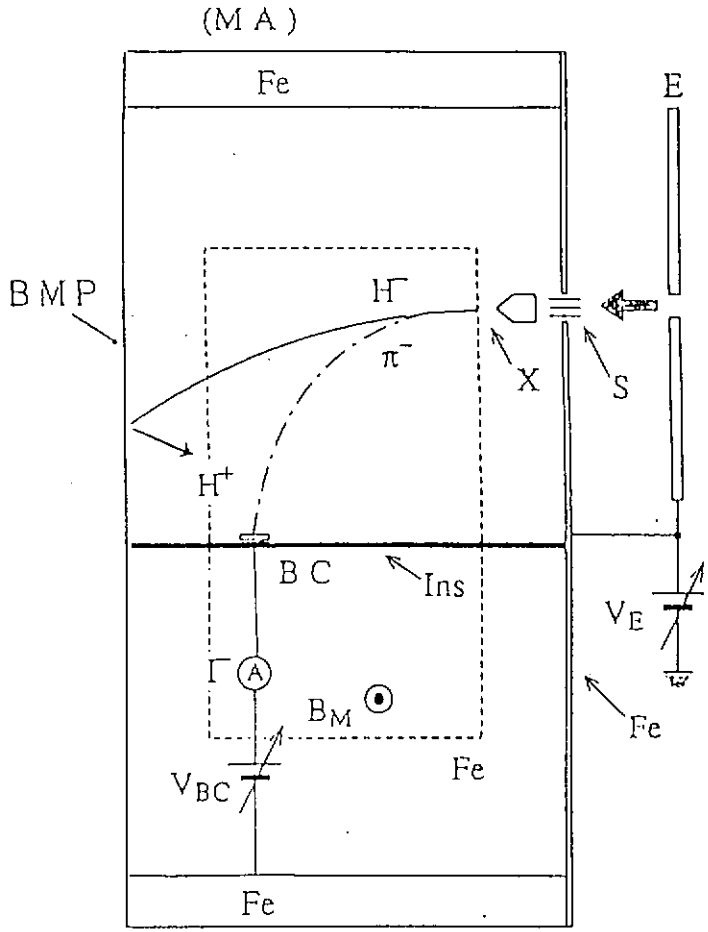
(M A)
Fe
E
BMP
H⁻
π⁻
X
S
H⁺
BC
Ins
VE
Γ
A
BM
Fe
VBC
Fe

(A)

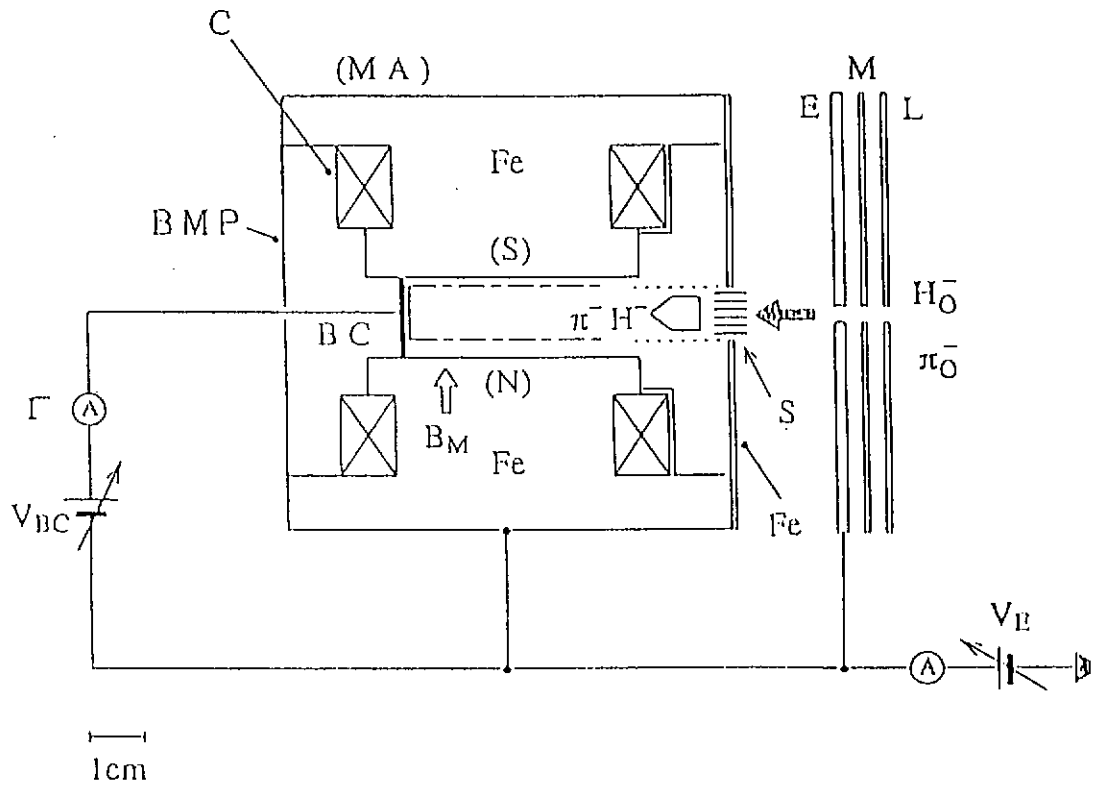
C
(M A)
M
E
L
Fe
BMP
(S)
H⁻O
π⁻O
BC
π⁻ H⁻
(N)
Γ
A
BM
Fe
S
VBC
Fe
VE
1cm

(B)

Fig. 8

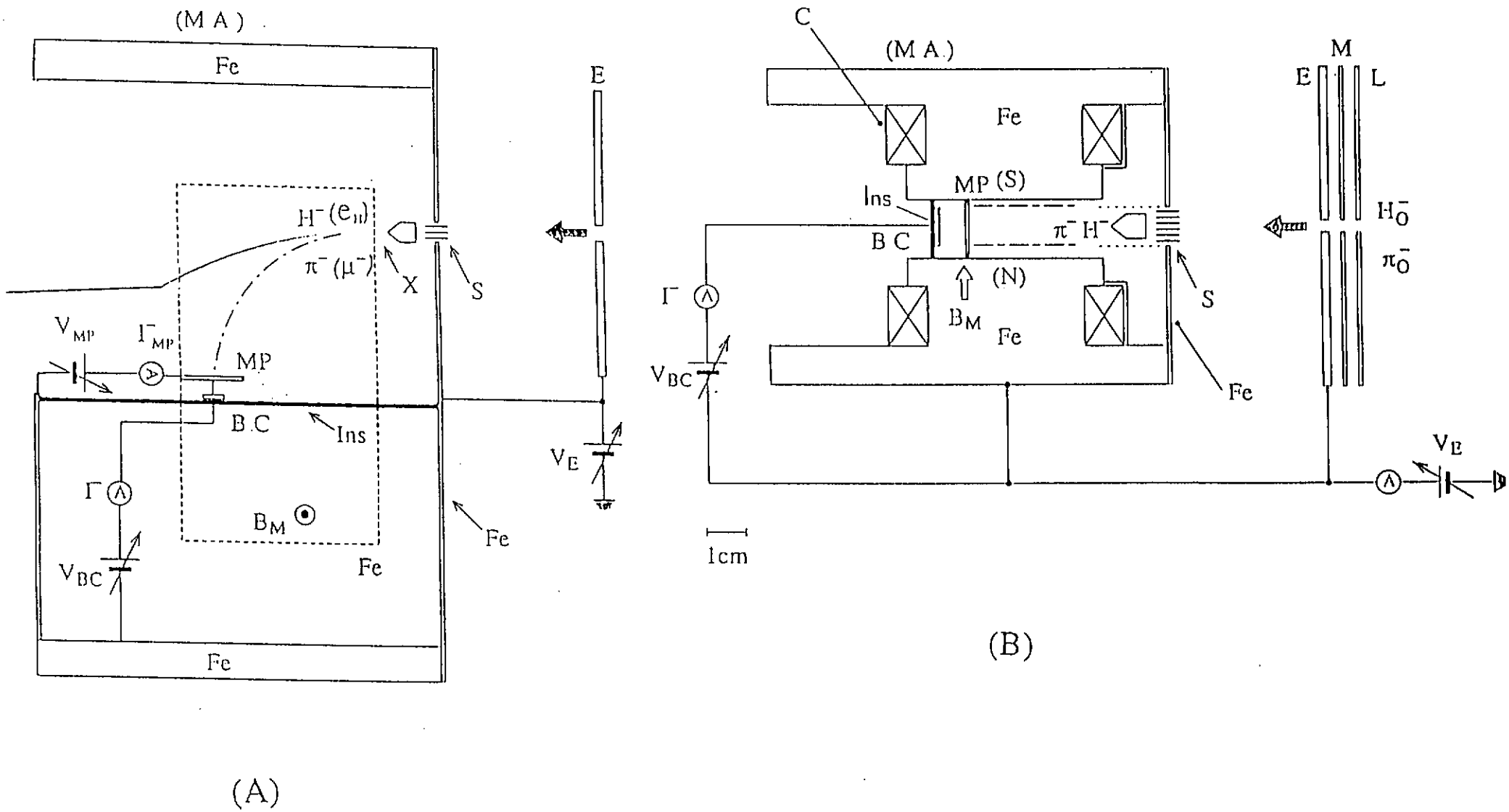
(M A)
Fe
E
H⁻ (e_II)
π⁻ (μ⁻)
X
S
V_MP
I⁻_MP
MP
B C
Ins
Γ
B_M
V_BC
Fe
Fe
Fe
V_E
(A)
C
(M A)
Fe
MP (S)
Ins
B C
π⁻ H⁻
(N)
B_M
Fe
S
Γ
V_BC
Fe
M
E
L
H⁻_O
π⁻_O
V_E
1cm
(B)

Fig. 9

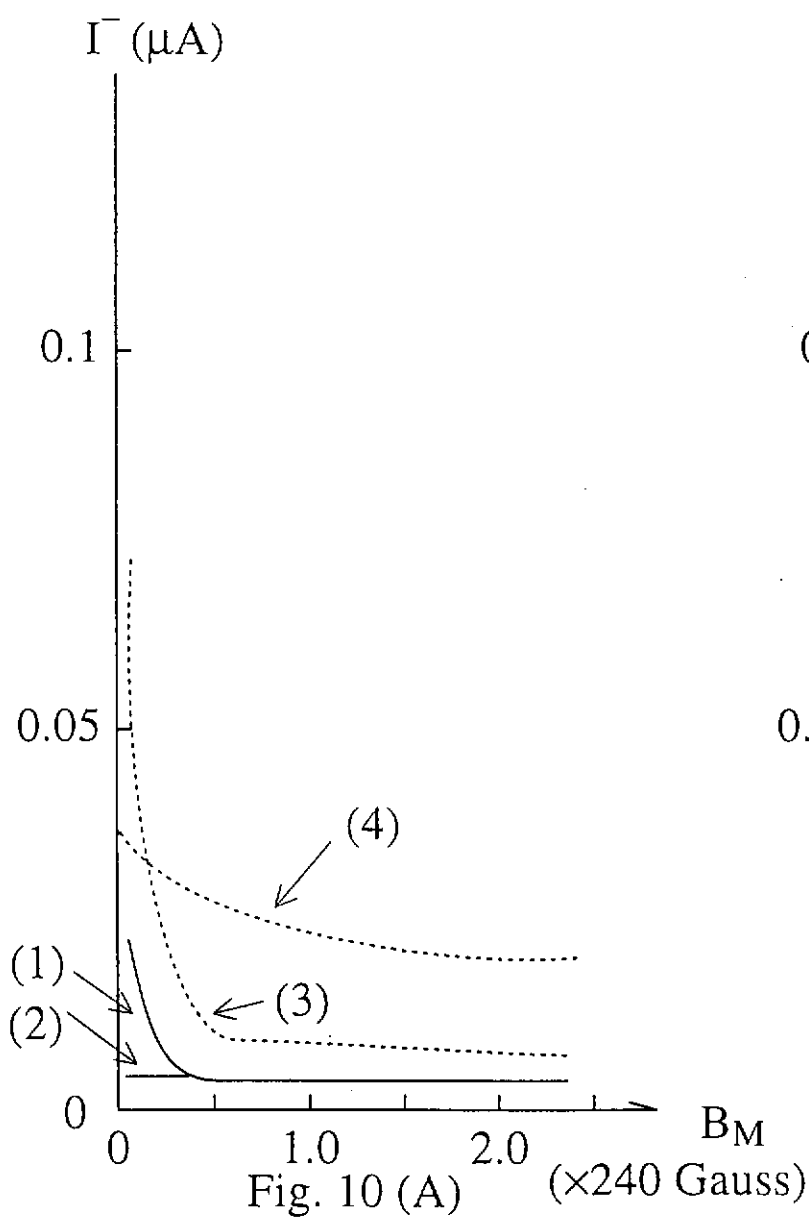

Fig. 10 (A)

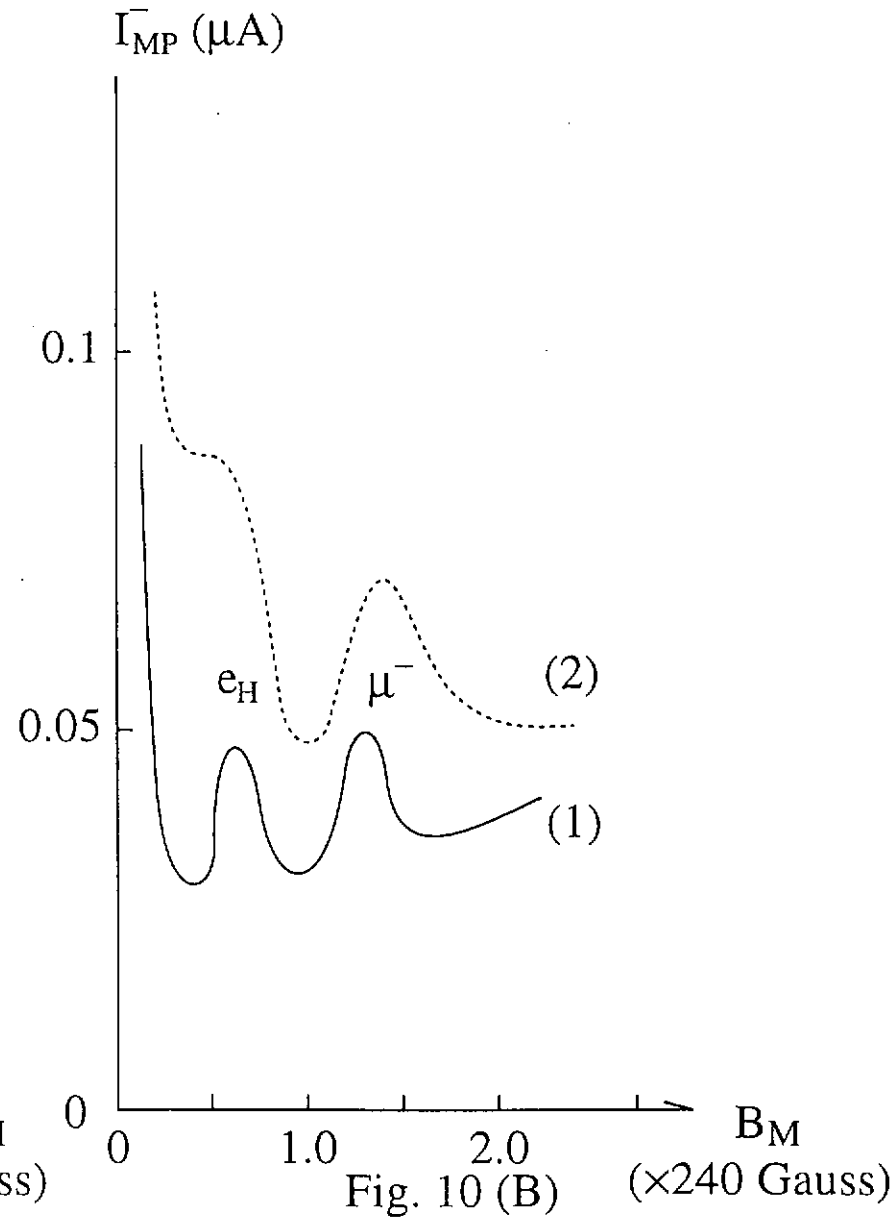

Fig. 10 (B)

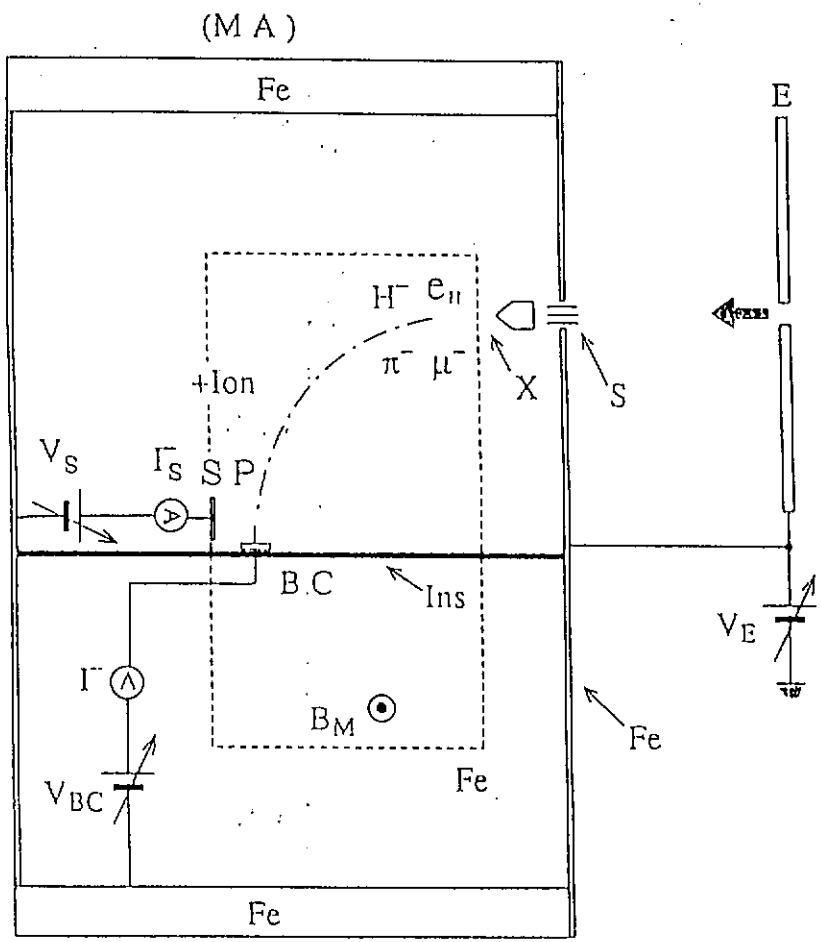
(M A)
Fe
E
H⁻ e
π⁻ μ⁻
+Ion
X
S
V_S
Γ_S
S P
B C
Ins
V_E
I⁻
B_M
Fe
V_BC
Fe

(A)

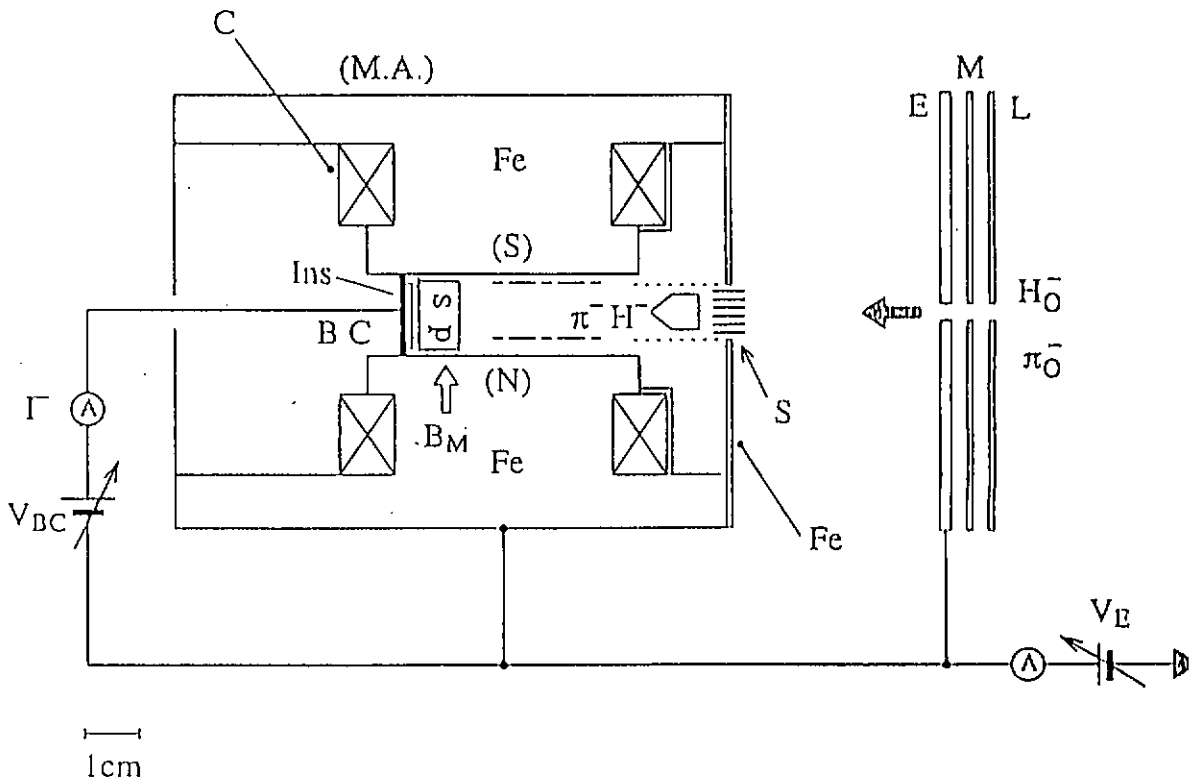
C
(M.A.)
Fe
(S)
Ins
B C
S P
π⁻ H⁻
(N)
B_M
Fe
Γ
V_BC
S
Fe
M
E
L
H⁻₀
π⁻₀
V_E
1cm

(B)

Fig. 11

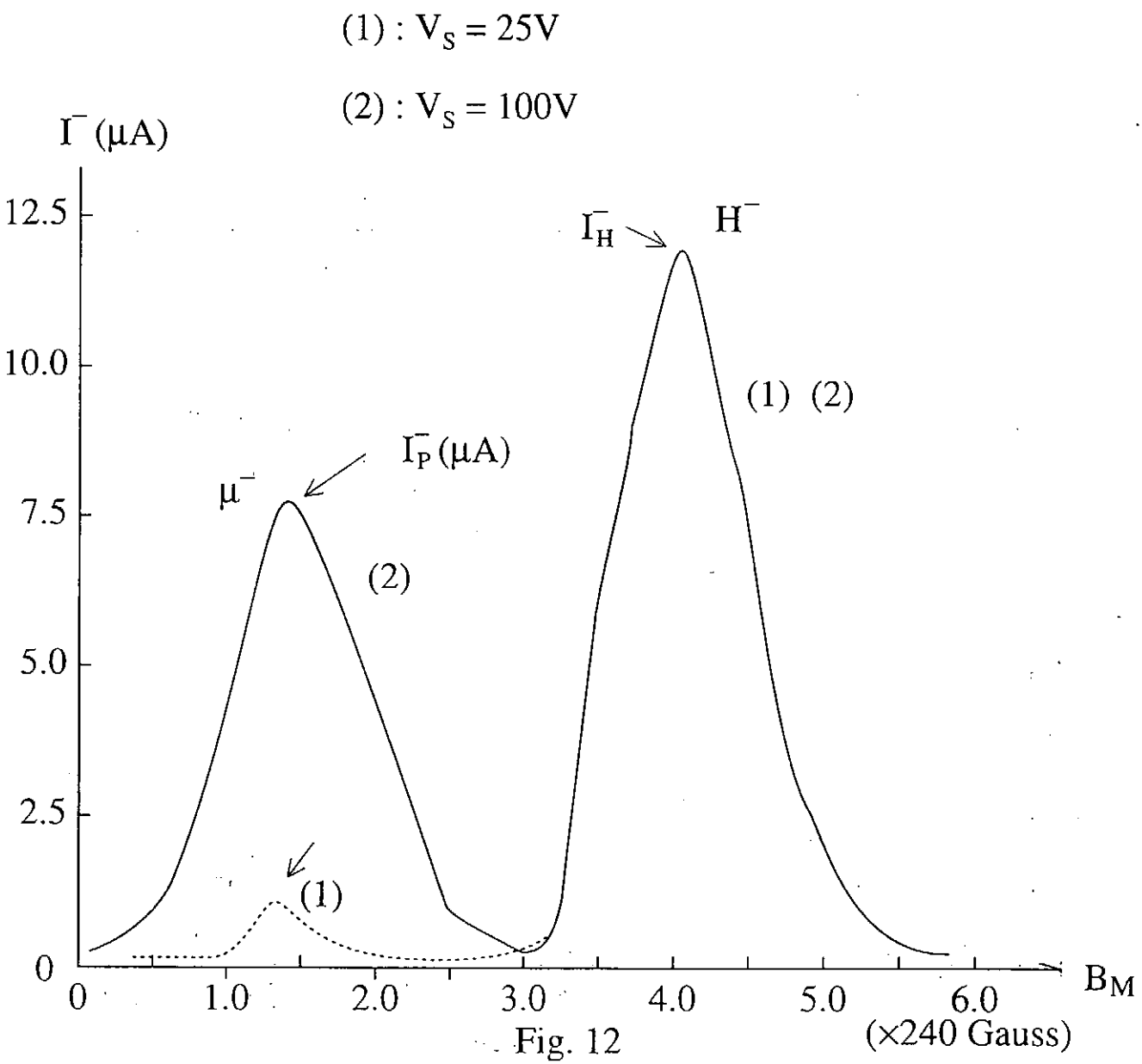
(1) : V_S = 25V
(2) : V_S = 100V
I^- (μA)
12.5
10.0
7.5
5.0
2.5
0
I_H^-
H^-
(1) (2)
I_P^- (μA)
μ^-
(2)
(1)
0
1.0
2.0
3.0
4.0
5.0
6.0
B_M
(×240 Gauss)

Fig. 12

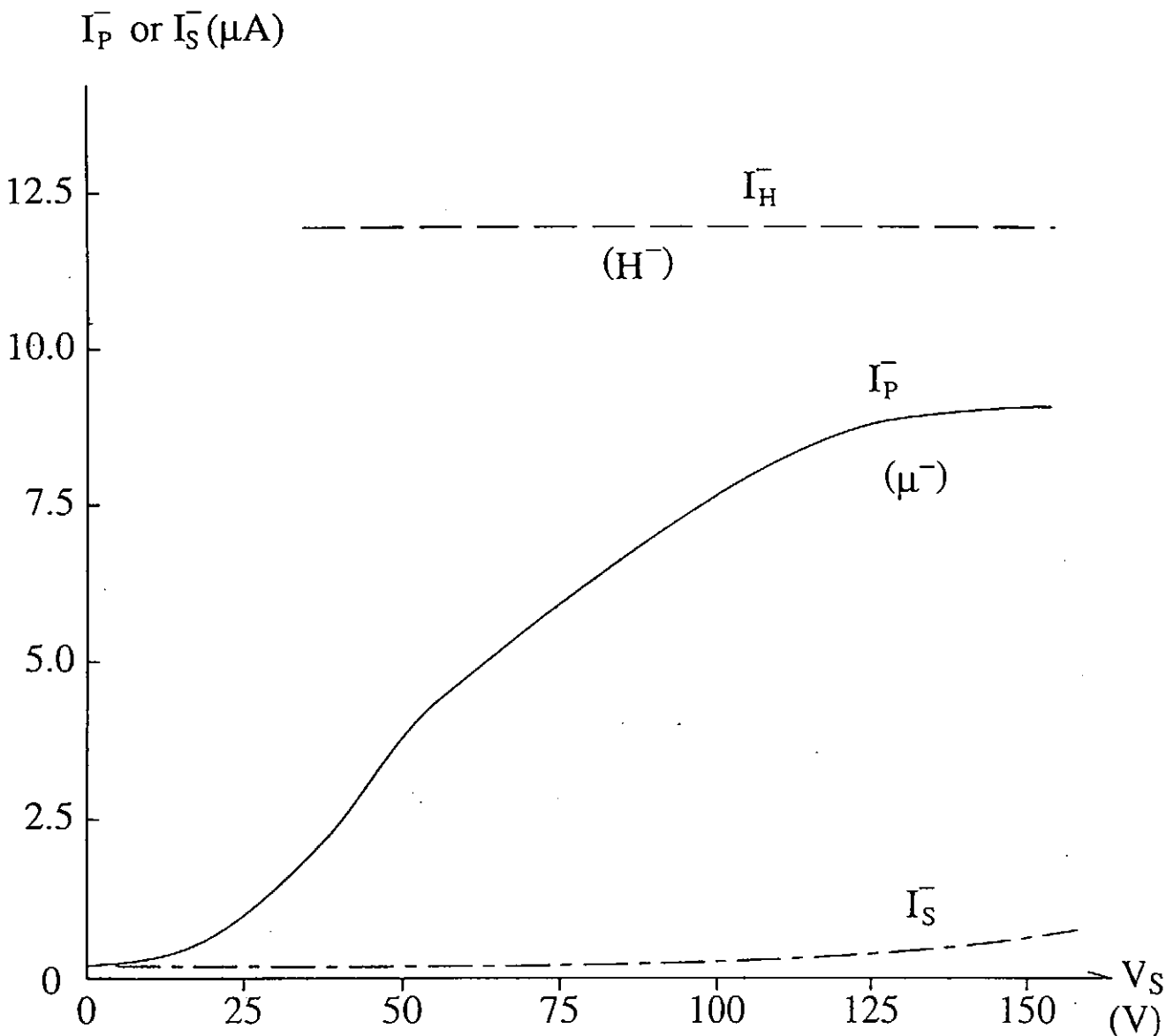

Fig. 13

Recent Issues of NIFS Series

NIFS-492 K. Ichiguchi, N. Nakajima, M. Okamoto,
Bootstrap Current in the Large Helical Device with Unbalanced Helical Coil Currents: Apr. 1997

NIFS-493 S. Ishiguro, T. Sato, H. Takamaru and The Complexity Simulation Group,
V-shaped dc Potential Structure Caused by Current-driven Electrostatic Ion-cyclotron Instability: May 1997

NIFS-494 K. Nishimura, R. Horiuchi, T. Sato,
Tilt Stabilization by Energetic Ions Crossing Magnetic Separatrix in Field-Reversed Configuration; June 1997

NIFS-495 T. -H. Watanabe and T. Sato,
Magnetohydrodynamic Approach to the Feedback Instability: July 1997

NIFS-496 K. Itoh, T. Ohkawa, S. -I.Itoh, M. Yagi and A. Fukuyama
Suppression of Plasma Turbulence by Asymmetric Superthermal Ions; July 1997

NIFS-497 T. Takahashi, Y. Tomita, H. Momota and Nikita V. Shabrov,
Collisionless Pitch Angle Scattering of Plasma Ions at the Edge Region of an FRC; July 1997

NIFS-498 M. Tanaka, A.Yu Grosberg, V.S. Pande and T. Tanaka,
Molecular Dynamics and Structure Organization in Strongly-Coupled Chain of Charged Particles; July 1997

NIFS-499 S. Goto and S. Kida,
Direct-interaction Approximation and Reynolds-number Reversed Expansion for a Dynamical System; July 1997

NIFS-500 K. Tsuzuki, N. Inoue, A. Sagara, N. Noda, O. Motojima, T. Mochizuki, T. Hino and T. Yamashina,
Dynamic Behavior of Hydrogen Atoms with a Boronized Wall; July 1997

NIFS-501 I. Viniar and S. Sudo,
Multibarrel Repetitive Injector with a Porous Pellet Formation Unit; July 1997

NIFS-502 V. Vdovin, T. Watari and A. Fukuyama,
An Option of ICRF Ion Heating Scenario in Large Helical Device; July 1997

NIFS-503 E. Segre and S. Kida,
Late States of Incompressible 2D Decaying Vorticity Fields; Aug. 1997

NIFS-504 S. Fujiwara and T. Sato,
Molecular Dynamics Simulation of Structural Formation of Short Polymer Chains; Aug. 1997

NIFS-505 S. Bazdenkov and T. Sato
Low-Dimensional Model of Resistive Interchange Convection in Magnetized Plasmas; Sep. 1997

NIFS-506 H. Kitauchi and S. Kida,
Intensification of Magnetic Field by Concentrate-and-Stretch of Magnetic Flux Lines; Sep. 1997

NIFS-507 R.L. Dewar,
Reduced form of MHD Lagrangian for Ballooning Modes; Sep. 1997

NIFS-508 Y.-N. Nejoh,
Dynamics of the Dust Charging on Electrostatic Waves in a Dusty Plasma with Trapped Electrons; Sep.1997

NIFS-509 E. Matsunaga, T.Yabe and M. Tajima,
Baroclinic Vortex Generation by a Comet Shoemaker-Levy 9 Impact; Sep. 1997

NIFS-510 C.C. Hegna and N. Nakajima,
On the Stability of Mercier and Ballooning Modes in Stellarator Configurations; Oct. 1997

NIFS-511 K. Orito and T. Hatori,
Rotation and Oscillation of Nonlinear Dipole Vortex in the Drift-Unstable Plasma; Oct. 1997

NIFS-512 J. Uramoto,
Clear Detection of Negative Pionlike Particles from H_2 Gas Discharge in Magnetic Field; Oct. 1997

NIFS-513 T. Shimozuma, M. Sato, Y. Takita, S. Ito, S. Kubo, H. Idei, K. Ohkubo, T. Watari, T.S. Chu, K. Felch, P. Cahalan and C.M. Loring, Jr,
The First Preliminary Experiments on an 84 GHz Gyrotron with a Single-Stage Depressed Collector; Oct. 1997

NIFS-514 T. Shimozuma, S. Morimoto, M. Sato, Y. Takita, S. Ito, S. Kubo, H. Idei, K. Ohkubo and T. Watari,
A Forced Gas-Cooled Single-Disk Window Using Silicon Nitride Composite for High Power CW Millimeter Waves; Oct. 1997

NIFS-515 K. Akaishi,
On the Solution of the Outgassing Equation for the Pump-down of an Unbaked Vacuum System; Oct. 1997

NIFS-516 *Papers Presented at the 6th H-mode Workshop (Seeon, Germany)*; Oct. 1997

NIFS-517 John L. Johnson,
The Quest for Fusion Energy; Oct. 1997

NIFS-518 J. Chen, N. Nakajima and M. Okamoto,
Shift-and-Inverse Lanczos Algorithm for Ideal MHD Stability Analysis; Nov. 1997

NIFS-519 M. Yokoyama, N. Nakajima and M. Okamoto,
Nonlinear Incompressible Poloidal Viscosity in L=2 Heliotron and Quasi-Symmetric Stellarators; Nov. 1997

NIFS-520 S. Kida and H. Miura,
Identificaiton and Analysis of Vortical Structures; Nov. 1997

NIFS-521 K. Ida, S. Nishimura, T. Minami, K. Tanaka, S. Okamura, M. Osakabe, H. Idei, S. Kubo, C. Takahashi and K. Matsuoka,
High Ion Temperature Mode in CHS Heliotron/torsatron Plasmas; Nov. 1997

NIFS-522 M. Yokoyama, N. Nakajima and M. Okamoto,
Realization and Classification of Symmetric Stellarator Configurations through Plasma Boundary Modulations; Dec. 1997

NIFS-523 H. Kitauchi,
Topological Structure of Magnetic Flux Lines Generated by Thermal Convection in a Rotating Spherical Shell; Dec. 1997

NIFS-524 T. Ohkawa,
Tunneling Electron Trap; Dec. 1997

NIFS-525 K. Itoh, S.-I. Itoh, M. Yagi, A. Fukuyama,
Solitary Radial Electric Field Structure in Tokamak Plasmas; Dec. 1997

NIFS-526 Andrey N. Lyakhov,
Alfven Instabilities in FRC Plasma; Dec. 1997

NIFS-527 J. Uramoto,
Net Current Increment of negative Muonlike Particle Produced by the Electron and Posititve Ion Bunch-method; Dec. 1997

NIFS-528 Andrey N. Lyakhov,
Comments on Electrostastic Drift Instabilities in Field Reversed Configuraiton; Dec. 1997

NIFS-529 J. Uramoto,
Pair Creation of Negative and Positive Pionlike (Muonlike) Particle by Interaction between an Electron Bunch and a Positive Ion Bunch; Dec. 1997

NIFS-530 J. Uramoto,
Measuring Method of Decay Time of Negative Muonlike Particle by Beam Collector Applied RF Bias Voltage; Dec. 1997

NIFS-531 J. Uramoto,
Confirmation Method for Metal Plate Penetration of Low Energy Negative Pionlike or Muonlike Particle Beam under Positive Ions; Dec. 1997